Hindawi
Geofluids
Volume 2022, Article ID 4773250, 17 pages
https://doi.org/10.1155/2022/4773250

Research Article

Study on the Application of Gob-Side Entry Retaining via Roof Cutting under the Condition of a Hard Thick Roof

Daoyong Zhu,[1,2] Huyue Zhang,[1] and Yi Su[2]

[1]*College of Water & Architectural Engineering, Shihezi University, Shihezi, 832000, China*
[2]*School of Mechanics and Civil Engineering, China University of Mining & Technology, Beijing 100083, China*

Correspondence should be addressed to Yi Su; suyicumtb@126.com

Received 8 May 2022; Revised 18 June 2022; Accepted 27 June 2022; Published 28 July 2022

Academic Editor: Hao Wu

To solve the problem of instability and failure of a roadway in the Dianping coal mine working face under the condition of traditional gob-side entry retaining, a mechanical model was established for analysis. The reasons for the damage are as follows: (1) the mining height is high, and the hard thick old roof exhibits large space for rotation and subsidence; (2) the retained roadway includes a large section; and (3) the mining impact is strong, and the adaptability of traditional cable is poor. Therefore, the technologies of "roof-cutting type gob-side entry retaining" were proposed and the principle was analyzed. Numerical simulation analysis of displacement and stress field under two processes was performed. The results indicated that the peak value of side abutment pressure decreased from 20.54 to 18.24 MPa due to the roof cutting (a decrease of 11%). The advance stress was less than the stress value under traditional conditions. When compared with the traditional conditions, the deformation of the roadway decreased by more than 50%. Finally, field monitoring was performed, and the results showed that under the condition of roof cutting, the deformation corresponded to the most severe within the range of 30–80 m behind the working face. After 80 m, the deformation gradually stabilized, and the maximum convergence between the roof and floor was 210 mm. Along the inclined direction, the stress of the hydraulic support in the middle part was the highest, the stress in the uncut side was second highest, and that in the roof-cutting side was the lowest. The periodic weighting interval on the roof-cutting side was the highest, and the transverse influence range of the roof cutting along the working face corresponded to 29.5 m.

1. Introduction

Gob-side entry retaining (GSER) is currently the most widely used no-pillar mining technology in the global coal industry [1–5]. It can decrease the waste of coal resources, decrease the extraction ratio, and realize y-type ventilation. However, it also exhibits limitations. The surrounding rock structures formed by the implementation of this GSER technology, the coal wall, roadside filling body, and floor are generally subject to large concentrated stress; the deformation and damage problem is more prominent. In addition, the geological conditions of the roadway are complex, such as hard thick roof and large mining height; the damage problem will be more serious [6–8]. Therefore, this study considers a series of practical engineering problems due to a hard and thick roof, to examine the deformation mechanism of surrounding rock.

Many studies have been performed on the roadway surrounding rock deformation and failure problem. Tan et al. [9] developed a new type of "compressible" filling body to adapt to the rotary and subsidence of the overlying strata. Han et al. [10] studied the deformation mechanism of roof and roadside filling body under the roof cutting condition. Wang et al. [11] studied the stress state and the deformation failure mechanism of the GSER roof structure and put forward a support design method. Coggan et al. [12] and Yang et al. [13] analyzed the surrounding rock structure of gob-side entry under different geological conditions and put forward the resultant support scheme. The results of the study indicate that the treatment methods for the deformation problem under the condition of a hard roof can be approximately divided into three categories [14–17]. The first is the improvement of the material of the filling body to adapt to the roof deformation. The second is roof cutting via blasting.

The third category involves strengthening the support to mobilize the bearing characteristics of the surrounding rock structure and achieve the best coupling support effect. This can stabilize the deformation of the surrounding rock to a certain extent. However, the roadway generally needs to be repaired many times with the recovery of the working face and reuse of the remaining roadway, which entails time and economic costs (irrespective of the method of roadway protection). The problem of "given deformation" of the roof and the stress concentration on the roadway due to the bending and sinking of the hard and thick main roof still exists, and this cannot be fundamentally solved [3, 18]. Therefore, the study proposed a new type GSER by roof cutting to solve the problem of large deformation and stress concentration of the surrounding rock [19–21].

In this study, the GSER under the condition of hard and thick roof of the working face 200 of Dianping coal mine in Shanxi Province is considered as an example. Given the large deformation and failure of the filling body and surrounding rock of the retained roadway during the mining process, it is unable to meet the requirements of safe mining. Therefore, the study proposed the technology of GSER by roof cutting via investigating its deformation mechanism and determining the reason for surrounding rock failure and examining the control mechanism of the surrounding rock. Finally, as revealed by the numerical simulation and on-site monitoring to evaluate the effect of retaining roadway, the findings exhibit a certain theoretical and practical reference significance.

2. Project Overview

2.1. Engineering Geological Conditions. Dianping coal mine is located in Liliu mining area, Shanxi Province, China, as shown in Figure 1(a). The average buried depth is 460 m, the tendency length of the working face is 220 m, and the strike length is 1088 m. The average thickness of the coal seam is 2.8 m, and the average dip angle is 4°, which is the near-horizontal seam. As shown in Figure 1(b), traditional filling-type GSER is adopted for the first 200 m section of the crossheading although the deformation of the roadway is excessively high and the damage is significant. Figure 1(c) denotes the histogram of the roof and floor strata with a direct floor of 3.3 m thick sandy mudstone and an old floor of 2.8 m thick fine sandstone. From the bottom to top, the roof is 2.8 m thick sandy mudstone, 6.1 m thick limestone, 0.7 m thick sandy mudstone, 2.4 m thick coal interlayer, and 4.0 m thick medium sandstone.

Figure 1(d) shows the original support section. Six left-hand nonlongitudinal bolts with a size of $\Phi 20 \times 2200$ mm are arranged on the roof, and the row and line space is 940 $\times$ 800 mm. The row and line between anchor cables is 2350×1800 mm, and the length is 6.2 m. Three Φ 16×1600 mm left-hand nonlongitudinal cables with a row and line space of 1200×800 mm are arranged on the two ribs. The anchor net adopts a 10# wire metal mesh, and the mesh size is 50×50 mm.

2.2. Original Engineering Problem. Figure 2 shows the failure of surrounding rock under the condition of traditional GSER. Figure 2(a) shows the on-site damage of the filling body, Figure 2(b) shows the floor heave of the retained roadway, Figure 2(c) shows the deformation of the solid coal, and Figure 2(d) shows the deformation monitoring curve of the original retained roadway. The displacement curve shows that the deformation of surrounding rock is low and the deformation rate is low when the monitoring section is located 0–20 m away from the working face. When the monitoring section lags behind the working face by 20 m, the deformation increases sharply, meaning a short period of instability failure of the filling body occurs. Surrounding rock failure occurs in the early stage of filling body construction within a distance of 20–50 m behind the working face. This is mainly affected by mining and rotary subsidence of the overlying hard and thick rock stratum. The deformation of the local surrounding rock in a low range gradually develops into an irreversible large-scale damage until the retained roadway failure, and this does not satisfy the requirements of safe production.

2.3. Failure Mechanism Analysis of the Original Project

2.3.1. Deformation Analysis of the Filling Body. To solve the failure problems effectively, it is necessary to perform an in-depth examination of the deformation and failure mechanism of surrounding rock, determine the main causes of failure, and then propose the corresponding treatment measures. Based on the structural characteristics of surrounding rock on site, the mechanical model of retained roadway is established, as shown in Figure 3. According to the field engineering experience, when the working face advances, the gob cannot support the hard thick roof. At this time, the left end of the roof can be regarded as supported by the coal pillar and the roadside filling body, and the other end is suspended in the gob. For the rock stratum, in order to achieve a new equilibrium state, the hard thick roof rotates and sinks to the gob and then compresses the filling body, i.e., the stress deformation of the filling body. From the geometric relationship shown in the figure, the maximum compression of key block B is obtained as follows [3]:

$$\omega = \frac{l_0 \cdot \Delta h}{l} = \frac{(a + b + 0.5c) \cdot \Delta h}{l}. \tag{1}$$

In the formula, w denotes the compression in the filling body; l denotes the lateral fracture span of the key block B; Δh denotes the maximum subsidence of the main roof; and l_0 denotes the distance from the main roof fracture line at the solid coal side to the filling body center.

The lateral fracture span and subsidence of the key block B is expressed as follows [8, 20]:

$$l = \frac{2d}{17}\left[\sqrt{\left(10\frac{d}{s}\right)^2 + 102} - 10\frac{d}{s}\right], \tag{2}$$

$$\Delta h = h_1 + h_2(1 - k),$$

where s denotes the width of the working face; d denotes the periodic weighting interval; h_1 denotes the mining height; h_2

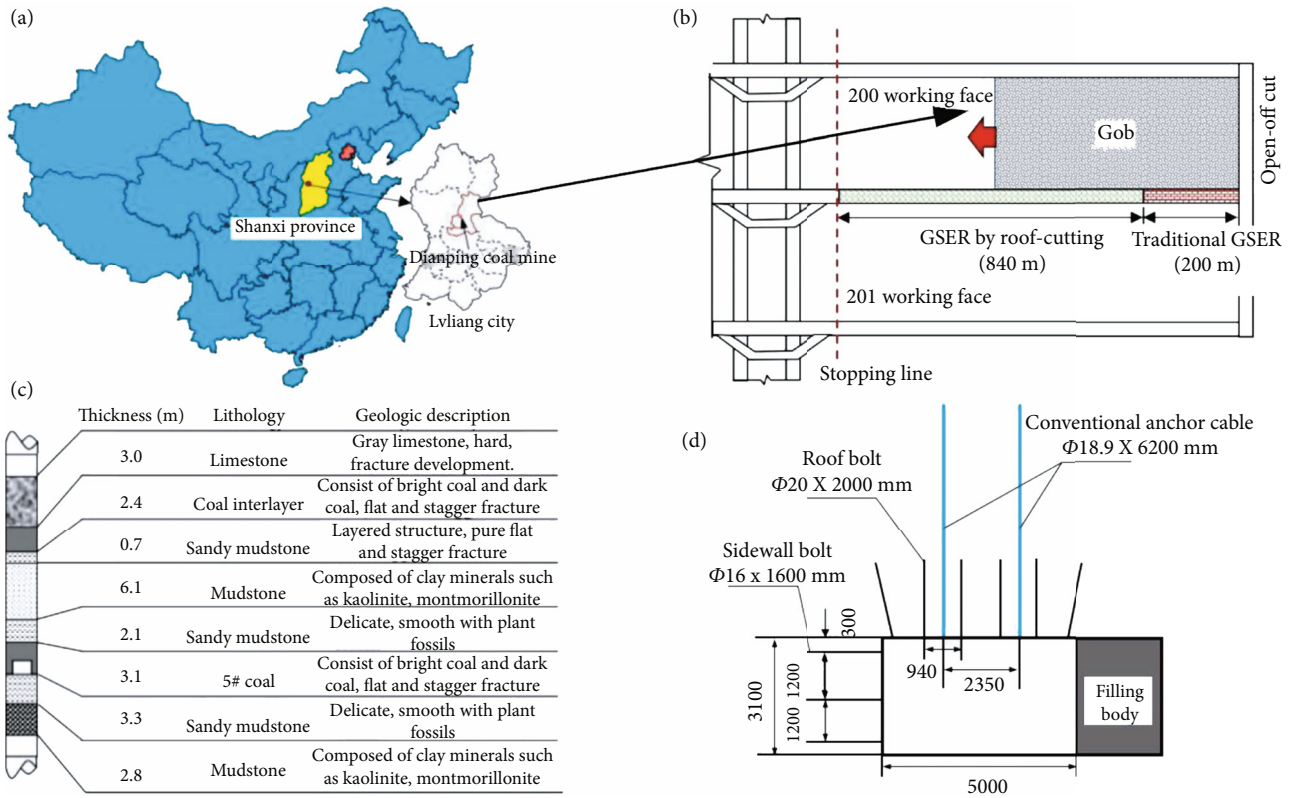

Figure 1: Project profile: (a) geographical position, (b) layout of the working face, (c) histogram of the roof and floor strata, and (d) original support section.

denotes the thickness of the direct roof, and k denotes the coefficient of bulk increase of the direct roof.

The above derivation and analysis indicate that the compression deformation of the filling body is related to the rotary subsidence of the hard thick roof, and its compression amount is generally related to the direct roof thickness and mining height. Decreases in the thickness of the direct roof and increases in the mining height increase the final subsidence of the basic roof and increase the compression amount of the filling body. When the filling body continues to be compressed and the deformation increases to a certain extent, the bearing capacity is lost resulting in instability failure, as shown in Figure 2(a). Further, the integrity of the roof is severely damaged.

2.3.2. Floor Deformation Analysis. Based on the uneven floor heave deformation shown in Figure 2(b), a mechanical model is established, as shown in Figure 4. The surrounding rock structure of the retained roadway is mainly composed of four parts: the roof, coal wall, roadside filling body, and floor. The roof can be regarded as a suspended beam supported by the coal wall and the filling body on both sides, subjected to its own gravity and the pressure of the overlying strata. The roadway on both sides is squeezed by the overlying strata. The floor is regarded as a squeezing effect formed by the pressure of the overlying strata transmitted to the floor through the coal slopes on both sides. Therefore, the two ends of the floor rock beam are considered as fixed ends, the overlying strata on the left side apply uniform stress to the floor beam via solid coal, and the filling body on the right end is considered as the uniformly increasing linear stress due to the compression of the old roof strata. The floor strata are considered as beam structures of unit thickness. Based on the analysis of the superposition principle of material mechanics, the stress model in Figure 4(b) is decomposed into the superposition of three mechanical models as shown in Figure 4(c). Therefore, the deflection deformation is calculated separately, and the final displacement of the floor rock beam is obtained by the superposition of the final results as follows [9]:

$$\omega = \frac{-\left\{\left((\sigma + k\gamma h)/2\right)c^5\left[2\left(x^2/c^2\right) - (x/c)\left(2\left(l^2/c^2\right) - 1\right)\right] + pa^5\left[2\left(\left(l - x'\right)^2/a^2\right) - \left(\left(l - x'\right)/a\right)\left(\left(2\left(l^2/a^2\right) - 1\right)\right)\right] + fxl\left(l^3 - 2lx + x^2\right)\right\}}{24EIL}, \tag{3}$$

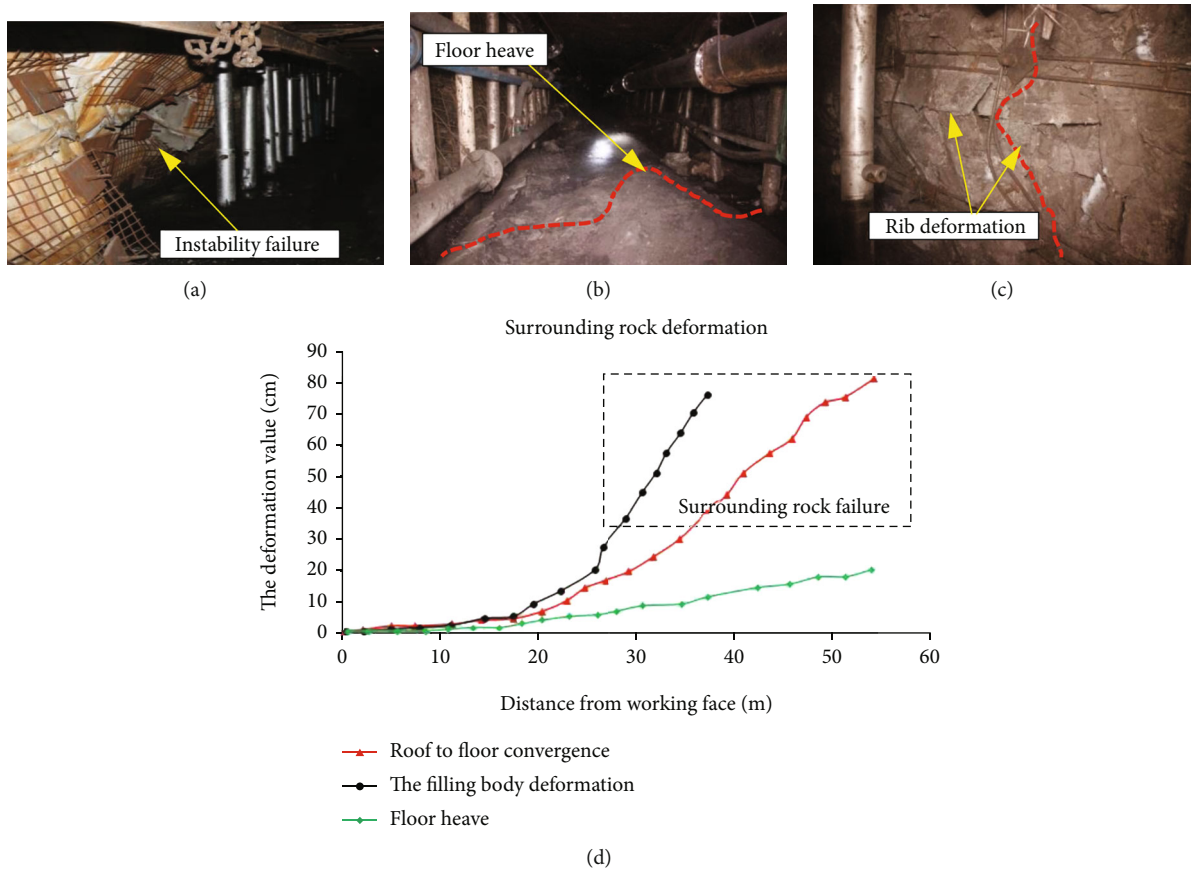

Figure 2: Failure under traditional gob-side entry: (a) failure of filling body, (b) floor heave, (c) solid coal deformation, and (d) deformation curve of the surrounding rock.

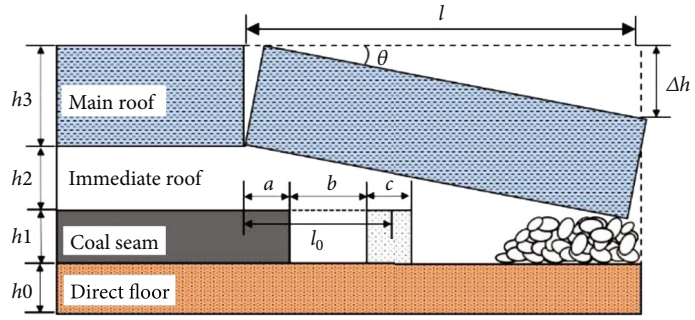

Figure 3: Mechanical model of gob-side entry retaining.

where a denotes the width of the solid coal side; b denotes the width of the roadway; c denotes the width of the filling body; p denotes the uniform stress applied on the floor of the solid coal side; $\sigma, \lambda\gamma h$ denotes the linearly increased stress at the right end; p denotes the uniform stress on the left end; f denotes the uniform stress on the reserved roadway floor; E denotes the elastic modulus of rock; and I denotes the moment of inertia.

The aforementioned mechanical analysis of the surrounding rock deformation along with the actual on-site damage indicates that there are four main reasons for the failure of the surrounding rock. First, the hard and thick old roof rotates and sinks, and this compresses the surrounding rock and filling body. Second, the mining height is relatively high and the direct roof is relatively thin. After coal mining, the filling height of gangue formed by the direct roof caving is relatively low, and the space from gangue layer to the basic roof is relatively high, thereby creating favorable conditions for the subsidence of hard and thick roof. Third, the retained roadway exhibits a large section, the direct roof is weak and easy to break, and the support is difficult. Fourth, with increases in the main roof periodic fracture length, the mine pressure appears violently, and this significantly affects the working face and retained roadway.

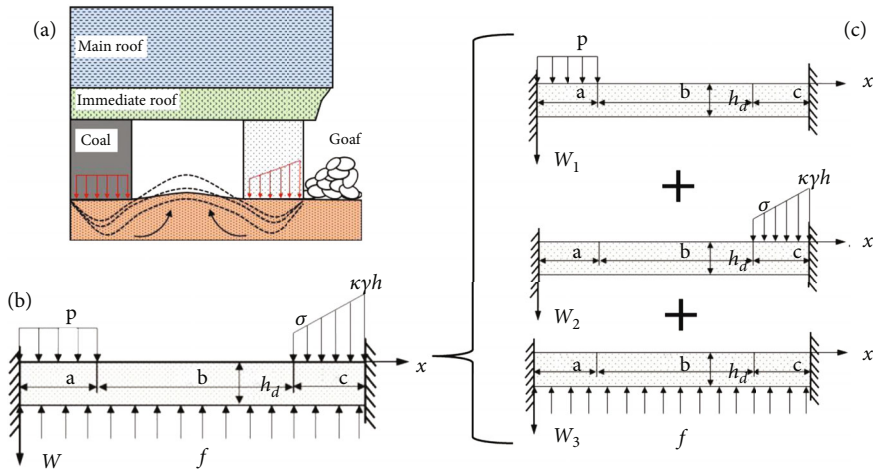

Figure 4: Mechanical analysis of the floor: (a) floor stress, (b) floor mechanical model, and (c) stress decomposition.

Furthermore, under the severe impact, it is easy for the traditional cable to slip and break, which further aggravates the deformation.

3. Control Measures

The main causes of roadway large deformation are the fracture of the main roof as its rotates and sinks, the breakage of the hard and thick main roof into articulated beam structure that transmits additional stress, and the instability of the traditional anchor cable under the effect of the surrounding rock deformation and mining impact. Therefore, given the specific problems, two ideas were proposed to solve the field problems. One idea involves manually cutting the roof such that the rock mass within the scope of roof cutting is easy to collapse, fill the goaf, support the upper rock layer, decrease the rotation and subsidence of the upper rock layer, cut off the articulated beam transmission structure formed by the main roof fracture, and optimize the stress distribution of the surrounding rock [17, 21]. The other idea involves using a new type of cable that is suitable for large deformation and exhibits better anti-impact performance for reinforcing the support in the retained roadway. Based on the aforementioned two control ideas, the study proposes a new roof-cutting-type GSER technology.

3.1. Gob-Side Entry Retaining by Roof Cutting. Figure 5(a) shows the layout of the GSER via roof cutting. There are three main steps in the technology. Figure 5(b) shows the first step, which involves strengthening the support with constant resistance and large deformation (CRLD) anchor cable based on the original support. After the support is completed, directional blasting is performed to cut the roof strata. There are two main parameters to be considered in the roof-cutting process. The first parameter is the cutting angle, which is generally determined by field construction and numerical simulation and generally does not exceed 25°. The other parameter corresponds to the roof-cutting height, as shown in Figure 5(b). We assume that there are n layers in the scope of the roof cutting, and the coefficient of bulk increase in each layer is $k_1, k_2, \cdots, k_n$. The thickness of each layer corresponds to $h_1, h_2, \cdots, h_n$. The roof-cutting height is obtained as follows [17]:

$$k_1h_1 + k_2h_2 + \cdots + k_nh_n \approx k_p \sum_{i=1}^{n} h_i. \tag{4}$$

The height of roof cutting is calculated as

$$H = \sum_{i=1}^{n} h_i = \frac{M}{k_p - 1}, \tag{5}$$

where H denotes the roof-cutting height; M denotes the mining height; and k_p denotes the coefficient of bulk increase of each layer.

The second step is shown in Figure 5(c). The lateral gangue retaining support is performed to prevent the collapsed rock mass from entering the retained area and from ensuring that the gangue becomes the rib of the roadway. The third step is shown in Figure 5(d). When the working face advances a certain distance, the movement of the overlying strata is completed, the surrounding rock of the retained roadway is stabilized, temporary support tools (such as the single hydraulic prop) are removed, and concrete is sprayed to isolate the goaf (which will be reused in the next working face).

The technology mainly uses the expansion property of fallen rock to make the cut-off rock fill the goaf, as shown in Figure 5(d). The filled rock exhibits a certain supporting capacity for the wedge-shaped pressure zone formed by the roof cutting above the retained roadway and the overlying strata near the roof-cutting line. When compared with the traditional GSER, it significantly decreases the rotary and subsidence of the overlying strata. Additionally, the articulated beam structure formed by the hard main roof above the retained roadway is cut off. The horizontal thrust between the rock beams cannot be transmitted to the retained roadway surrounding rock, which optimizes the

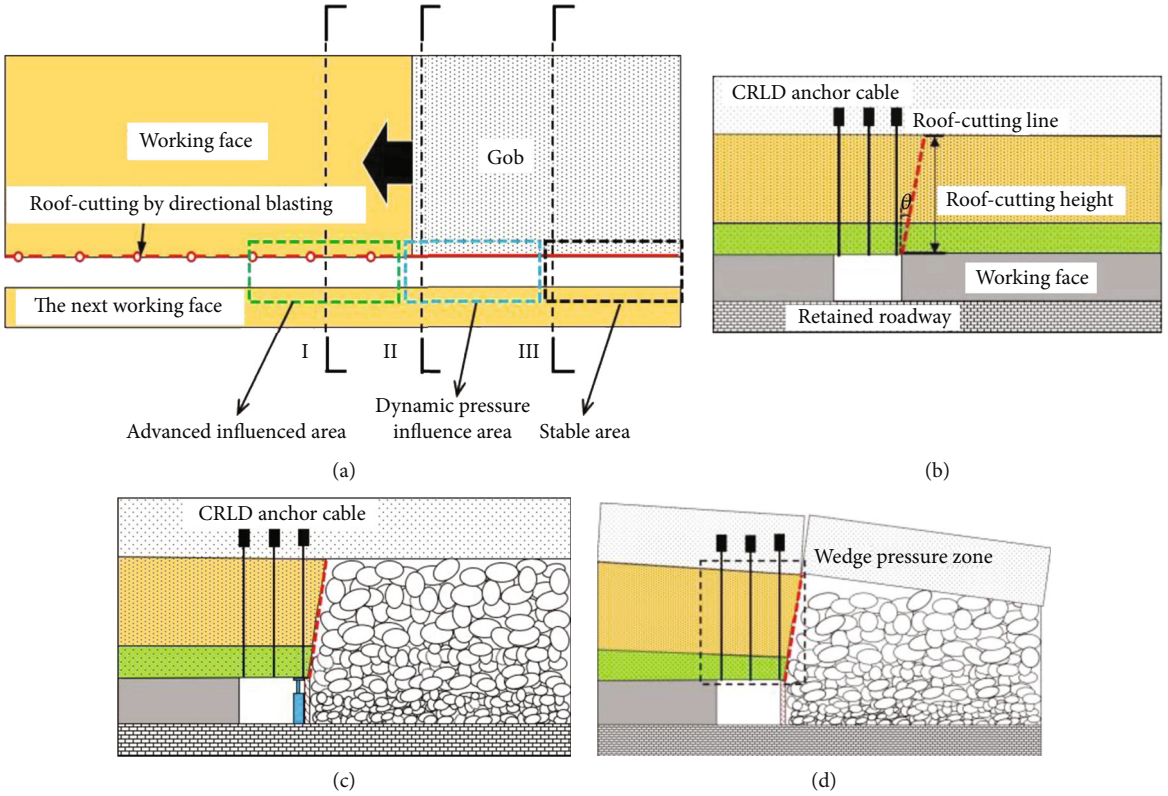

Figure 5: Gob-side entry retaining via roof cutting.

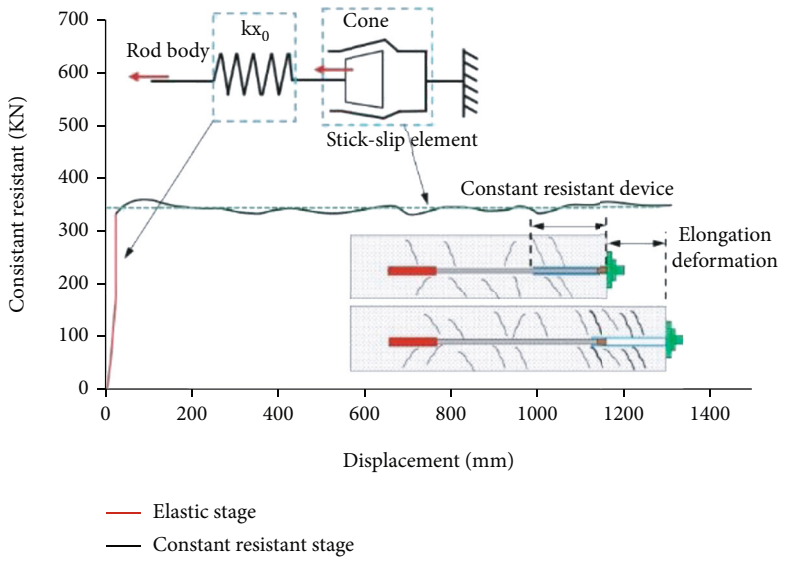

Figure 6: Principle of CRLD anchor cable support.

stress distribution and fundamentally solves the cause for the large deformation of the traditional roadway.

3.2. Analysis of Main Technical Principles

3.2.1. CRLD Anchor Cable Support. Figure 6 shows the working principle of the CRLD anchor cable. When the surrounding rock deformation is low, the elastic deformation of the anchor cable rod initially occurs, i.e., as denoted by the red stage of the stress displacement curve in Figure 6. The displacement in this stage is low, although the force of the cable increases sharply. The force is expressed as follows [22]:

$$p = k_e x_e, \tag{6}$$

where p denotes the tensile force in the elastic stage of the anchor cable, k_e denotes the elastic constant, and x_e denotes the elastic elongation of the rod.

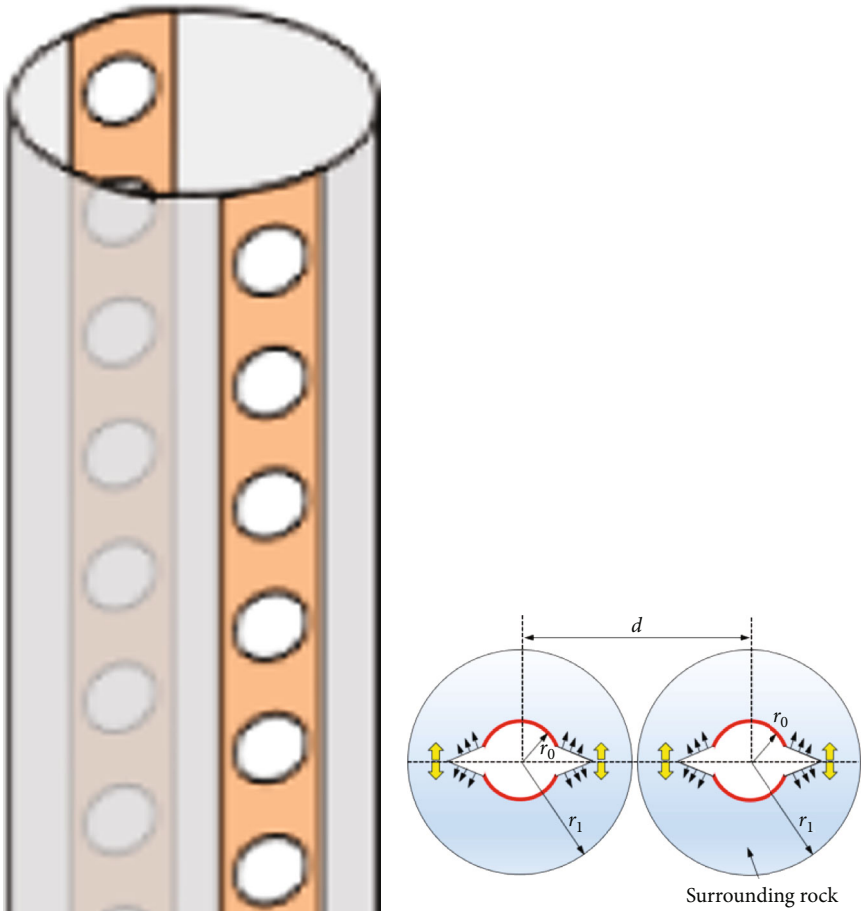

(a) (b)

Figure 7: Bidirectional cumulative tension blasting technology: (a) guide pipe; (b) principle of directional blasting.

With further increases in the surrounding rock deformation, when the stress of anchor cable increases to constant resistance, the cone slides in the sleeve to produce constant friction resistance. In this stage, the anchor cable can produce large displacement deformation under the condition of maintaining constant working resistance as follows [22]:

$$p = p_0, \tag{7}$$

where p_0 denotes the constant resistance.

As shown in Figure 5(a), the CRLD cable generally experiences the effect of deformation in multiple stages with advances in the working face including the initial mining deformation stage, mining influence stage of the working face, and reuse stage of the remaining roadway. Currently, the elongation deformation rate of ordinary mine anchor cable is generally between 3% and 5%. Additionally, after the tension deformation, with increases in deformation, the support strength and impact resistance of the traditional bolt significantly decrease, and this does not satisfy the requirements of roadway safety. However, the CRLD anchor cable can overcome the disadvantage. It exhibits the characteristics of large deformation. The elongation deformation can generally reach 1000 mm. It can maintain a constant high support strength under the condition of large deformation or strong impact. Therefore, CRLD cable reinforcement is an important technology in this process.

3.2.2. Roof Cutting by Directional Blasting. To ensure that the overlying rock collapses smoothly, directional blasting technology (also known as bidirectional cumulative tension blasting technology) is performed. As shown in Figure 7(a), the guide hole is excavated in advance, and the guide pipe with two rows of round holes is installed in the hole. The guide hole increases the auxiliary free surface of blasting in the direction of the aperture [23]. When the blast stress wave propagates to the free surface, it is reflected as a tensile wave. When the tensile wave exceeds the tensile strength of the surrounding rock mass, the rock mass falls from the free side to the inner side. Simultaneously, the reflected tensile wave and stress field at the tip of the radial fracture are superposed, thereby causing the fracture to spread further along the set direction and forming an effective fracture surface.

When the total tensile stress strength after stress superposition exceeds the tensile strength of the rock mass, the initial crack is generated and expands along the direction of the guide hole until the tensile stress is less than the ultimate tensile strength of the rock mass. The process is expressed in Formula (10) as follows [17]:

$$\left(1 + \frac{A_2}{A_1} + \frac{C_s A_{sv}}{C_p A_1}\right)\sigma_y \geq \sigma_r, \tag{8}$$

where A_1, A_2, and A_{sv} denote the amplitudes of incident P-wave, reflected P-wave, and reflected S-wave, respectively; C_s and C_p denote the velocities of P-wave and S-wave, respectively; σ_y denotes the strength of the stress wave (formed by the explosion of the explosive in the rock mass) propagating to the control hole wall, and σ_r denotes the dynamic tensile strength of the rock mass.

Based on the attenuation law of stress wave in rock mass, the calculation formula of blasting stress damage range r_1 is expressed as follows [17]:

$$r_1 = r_0\left\{\frac{\left[bp_2\left(1 + (A_2/A_1) + \left(C_s A_{sv}/C_p A_1\right)\right)\right]}{\sigma_r}\right\}^{1/a}, \tag{9}$$

where r_0 denotes the radius of the blasting hole; a denotes the intensity attenuation index of stress wave; b denotes the tensile stress coefficient; and p_2 denotes the reflection angle of the reflected longitudinal wave.

Therefore, in order to obtain a good roof-cutting effect, the fractures should be connected to form an effective blasting surface as shown in Figure 7(b), and distance d between the two holes should exceed the sum of the damage radius generated by the blasting as follows:

$$d \leq 2(r_0 + r_1). \tag{10}$$

Therefore, Formulas (11) and (12) can be used as the basis of charge design and blast hole design, respectively.

3.2.3. Lateral Gangue Retaining Technology. After the working face is mined, in order to prevent the collapsed rock mass from flowing to the retained roadway area, the "single hydraulic prop + joist steel + steel mesh" is used for support along the roof-cutting line. As shown in Figure 8, the overlying rock mass in the goaf gradually collapses, and the process exhibits certain timeliness, which can be considered as the dynamic evolution process of "collapse→ compaction→ stability." Furthermore, the collapse and accumulation of the rock mass show the dynamic impact of the gangue on the retaining structure while the compaction shows the transverse extrusion on the retaining structure. Gao et al. [19] simplified the collapsed gangue into a rigid sphere with uniform mass (Figure 8(b)), simplified the collapse stage of the rock mass into the leaping movement along the slope, and deduced the speed of the gangue impacting the retaining structure as follows [19]:

$$v_g = \sqrt{2gH\cos^2\beta + \left[gH\sin\left(2\beta + x_M - x_0\right)\right]^2 \frac{2H\cos^2\beta}{g}}, \tag{11}$$

where H denotes the initial height difference between the gangue and stacked slope and x_0 denotes the initial position when the gangue impacts the slope. Additionally, β denotes the angle between the direction of the gangue movement speed and horizontal line.

According to Guo et al. [24], based on the limit equilibrium method (Figure 8(d)), the lateral pressure at any

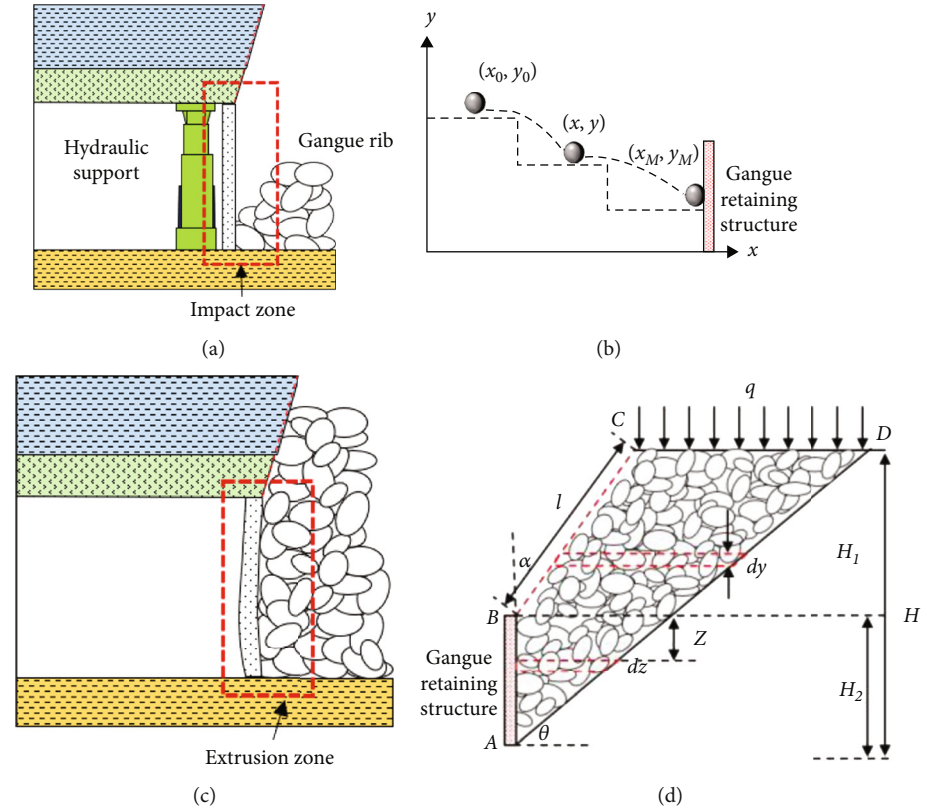

Figure 8: Mechanical model of the retaining gangue: (a) collapse stage of gangue, (b) mechanical model of collapse stage, (c) stable stage of gangue rib, and (d) mechanical model of stability stage.

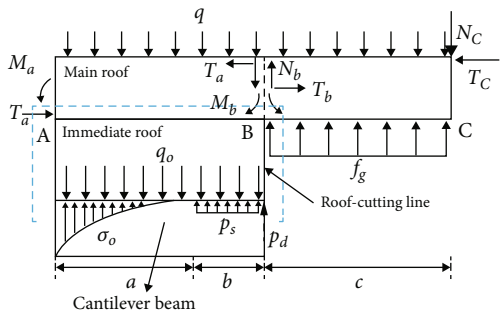

Figure 9: Mechanical model of support resistance.

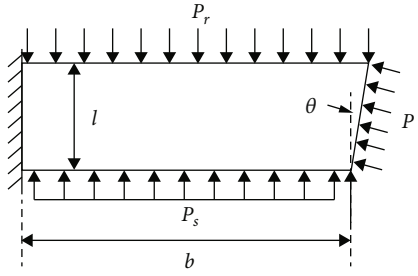

Figure 10: Mechanical model of cantilever beam.

position of the retaining structure in the stable stage is derived as follows [24]:

$$\begin{cases} \sigma_h = k_{a2}\left[\left(q_1 - \dfrac{\gamma H_2}{\xi_1 k_{a2} - 2}\right)\left(\dfrac{H_2 - z}{H_2}\right)^{\xi_1 k_{a2} - 1} + \dfrac{\gamma(H_2 - z)}{\xi_1 k_{a2} - 2}\right], \\ \xi_1 = \dfrac{\sin\theta\cos(\theta - \varphi - \delta_2)}{\cos\theta\cos\delta_2\sin(\theta - \varphi)}, \end{cases} \tag{12}$$

where δ_2 denotes the friction angle between the support structure surface and the gangue (°); k_{a2} denotes the coefficient of lateral pressure; and ξ_1 denotes the coefficient.

The analysis of gangue mechanical model in combination with the geological parameters to be examined approximately estimates the impact and lateral pressure on the retaining structure from the collapse to the stable stage and provides important theoretical guidance for the design of the retaining structure.

3.3. Mechanical Model. After roof cutting, the surrounding rock structure of the original GSER changed fundamentally, and the deformation mechanism of the surrounding rock also changed. Based on Figure 5(d), we establish a new mechanical model of GSER, as shown in Figure 8, and solve the support resistance and deformation via the solution of material mechanics. The assumptions are as follows: (1)

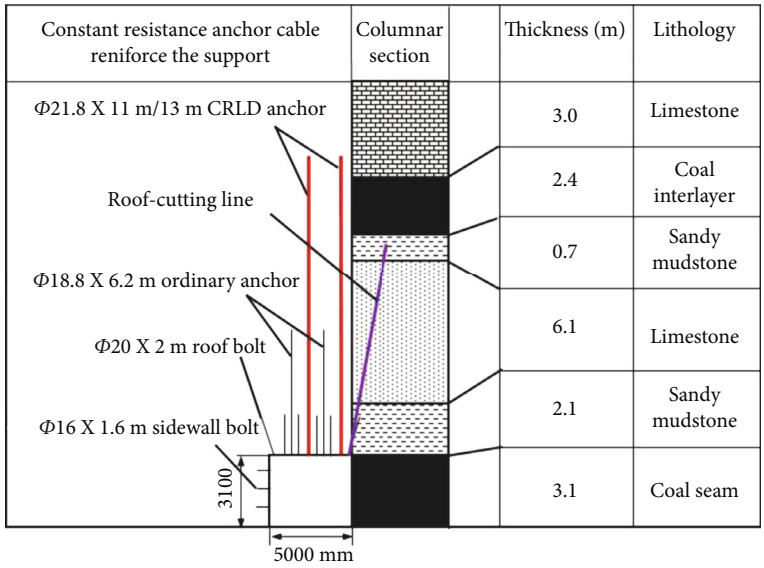

Figure 11: Support design.

the caved gangue provides uniform support force to the main roof; (2) shear force between the layers is zero; (3) old roof rotates and sinks to the goaf with the solid coal elastoplastic junction as the rotation axis; and (4) the roadway is subject to uniform support force, and the support force provided by the single pillar is simplified as a concentrated force [25, 26].

To solve the support resistance, for block *BC*,

$$\begin{cases} \sum F_y = 0, N_b + f_g \cdot c - qc - N_c = 0, \\ \sum F_x = 0, T_b = T_c, \\ \sum M_B = 0, M_b - \dfrac{1}{2} qe^2 - N_c \cdot c + T_c \left(\dfrac{h}{2} - \Delta S_c \right) + \dfrac{1}{2} f_g \cdot c^2 = 0. \end{cases} \tag{13}$$

It is concluded as follows:

$$N_c = \frac{M_b - (1/2)qe^2 + T_c((h/2) - \Delta S_c) + (1/2) f_g \cdot c^2}{c}. \tag{14}$$

For block AB,

$$\begin{cases} M_A = 0, \\ p_d(a+b) + \displaystyle\int_0^a \sigma_0 (a-x) dx + p_s b \left(a + \frac{b}{2} \right) + M_0 + T_b \left(\frac{h}{2} - \Delta S_B \right) - \frac{1}{2}(q+q_0)(a+b)^2 - N_b(a+b) - M_b = 0. \end{cases} \tag{15}$$

We substitute Equations (13), (14) into (15), and the support resistance under the condition of roof cutting is as follows [17]:

$$p_d = \frac{M_b + \left(N_c + qc - f_g c \right)(a+b) + (1/2)(q+q_0)(a+b)^2 - T_c((h/2) - \Delta S_B) - M_0 - \int_0^a \sigma_0 (a-x) dx - p_s b (a + (b/2))}{a+b}. \tag{16}$$

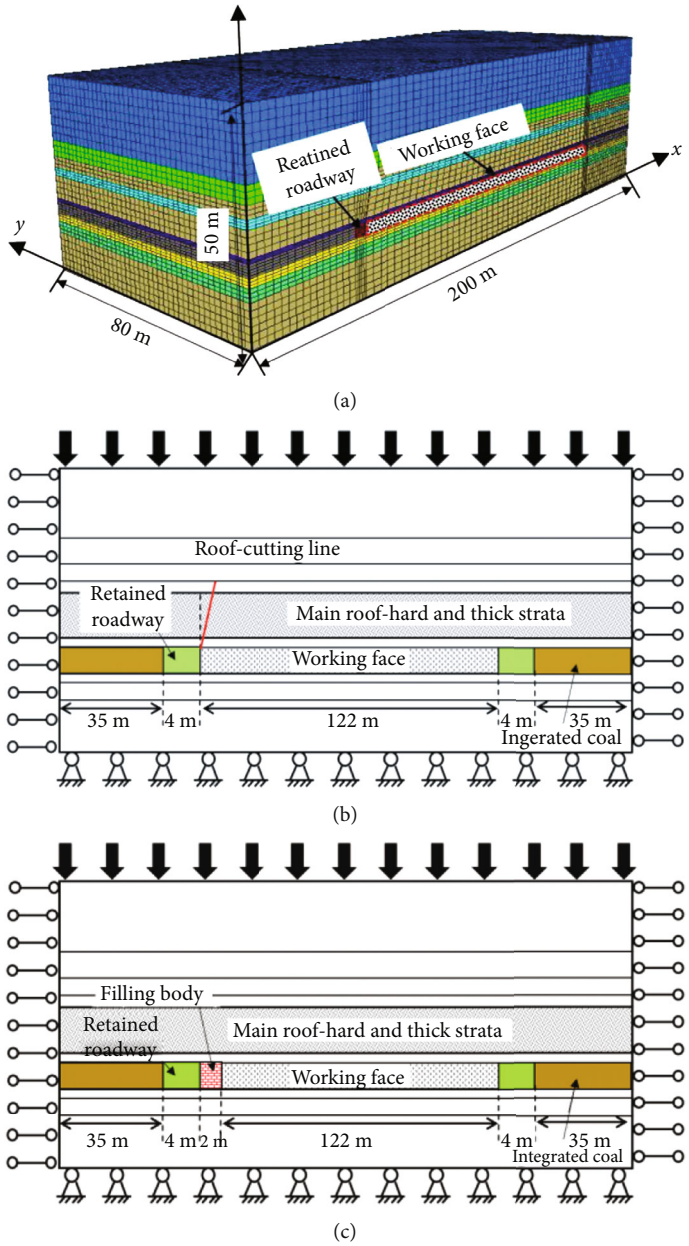

Figure 12: Numerical models and boundary conditions: (a) numerical model, (b) boundary conditions under roof cutting, and (c) traditional boundary conditions.

Here, p_d denotes the support resistance of single pillar; M_b denotes the ultimate bending moment of old roof; N_c denotes the shear force of old roof strata; f_g denotes the support force of gangue in goaf; q denotes the self-weight of unit length of the old roof and upper soft rock; q_0 denotes the self-weight of unit length of the direct roof; a denotes the width of limit equilibrium area; b denotes the width of roadway; c denotes the length of rock block BC; ΔS_c denotes the subsidence of end C when block AC is cut off; ΔS_B denotes the settling amount of end B; and h denotes the thickness of the old roof.

The dotted part in Figure 9 shows the cantilever beam structure formed by roof cutting. The left side denotes the fixed end, the right side denotes the free end, the upper boundary is considered the uniform weight of the overlying strata, and the lower boundary is considered as the uniform force of the roadway support. The mechanical model is shown in Figure 10.

The deflection deformation of the beam is solved, and the displacement deformation of the cantilever structure is obtained as follows [27]:

$$y = \frac{(p_r - p_s)x^2}{24EI}\left(6l^2 + x^2 - 4lx\right) - \frac{p\sin\beta x^2}{6EI}(3l - x). \quad (17)$$

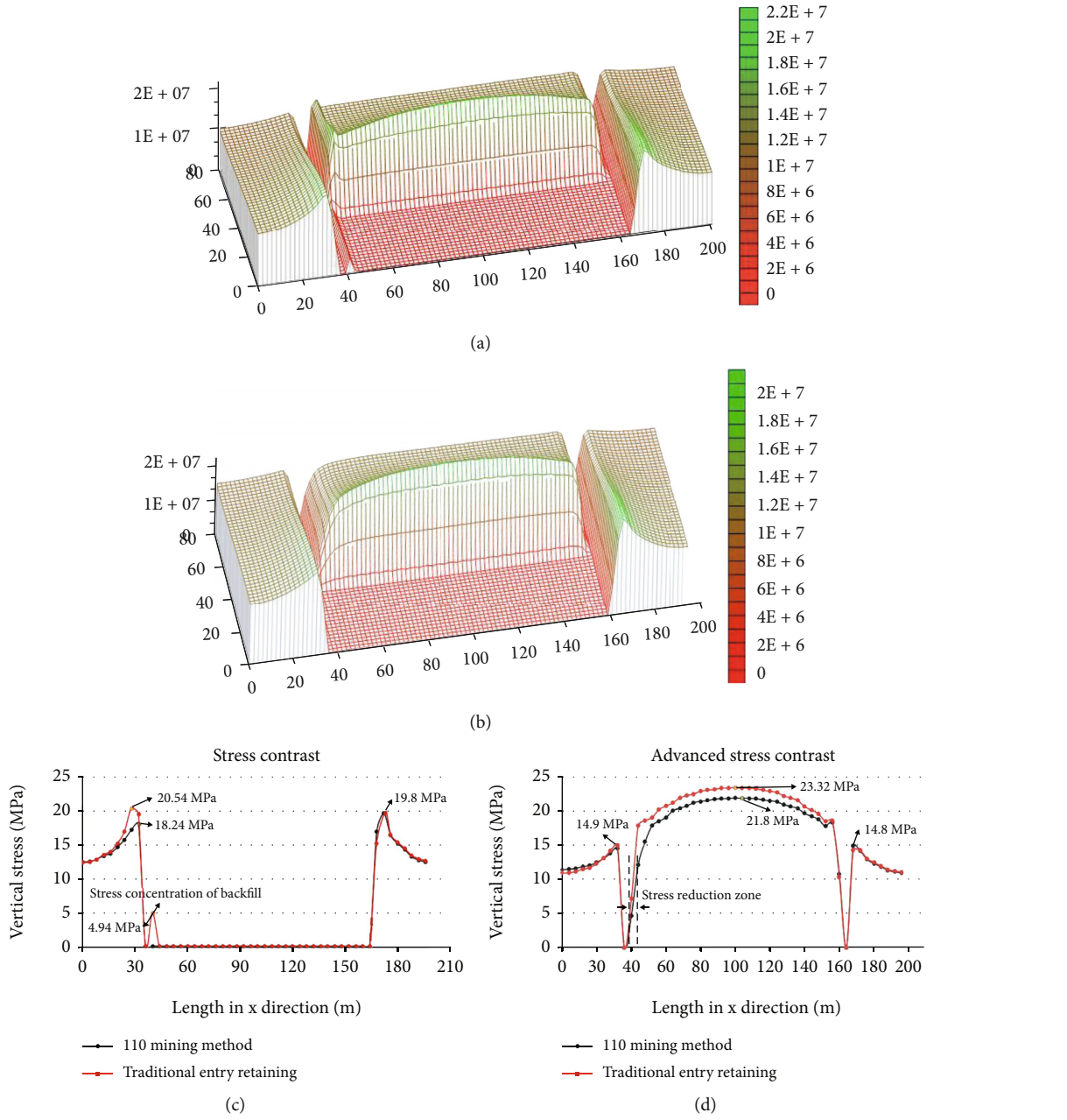

Figure 13: Law of stress evolution: (a) full field stress under traditional condition, (b) stress under the condition of roof cutting, (c) side abutment pressure comparison, and (d) advance stress comparison.

Therefore, the maximum displacement of the cantilever beam is obtained when $x = b$ as follows [22]:

$$y_{\max} = \frac{3(q_0 + \rho g - q_1)l^4 - 8F \sin \beta l^3}{24EI}. \quad (18)$$

Based on the analysis of the above mechanical model, it can be known that the support strength to ensure the stability of the roadway can be calculated from the mechanical model of the roadway support. Therefore, the strength of the bolt and anchor cable can be preliminarily determined in combination with the calculation of relevant field parameters. According to the calculation of the roof structure mechanical model, it can be concluded that the roof deformation at the roof cutting side is the largest, so the local reinforcement support design can be carried out in the field support design, and this provides a certain reference for roadway support.

3.4. Construction Design. The support design is performed based on the aforementioned theoretical design and research on retaining roadway. As shown in Figure 11, it corresponds to the support section of new retained roadway. Based on the original support, the CRLD anchor cable is used to reinforce the support, and it is arranged perpendicular to the roof with a total of two columns. The first row of CRLD cables is

Table 1: Physical and mechanical parameters of each lithology.

Lithology	Modulus of elasticity (GPa)	Shear modulus (GPa)	Cohesion (MPa)	Friction angle (°)	Density (kg/m^3)
Coal	5	1.9	0.8	30	1350
Sandy mudstone	9.1	6.5	1.3	32	2500
Medium sandstone	13.1	9.02	4.4	35	2400
Fine sandstone	10.6	7.3	2.9	30	2450
Limestone	17.9	11.52	6.2	37	2550

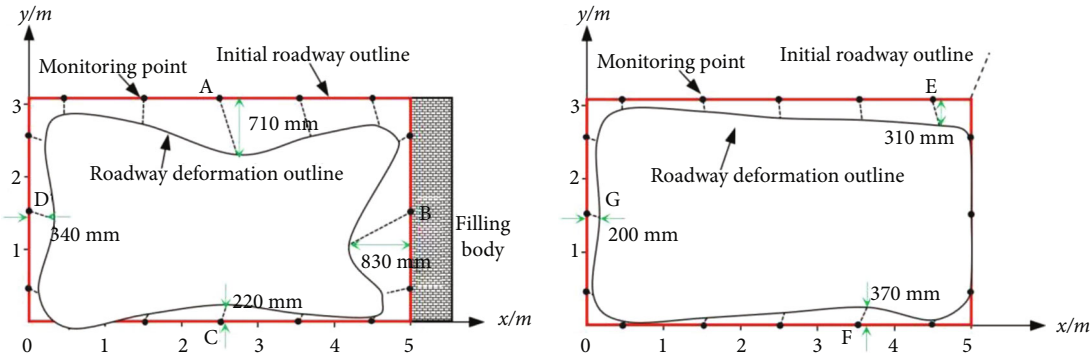

Figure 14: Deformation analysis of the retained roadway.

500 mm away from the roadway side, and the row spacing is 1000 mm. The second row is arranged in the middle of the roadway, and the row spacing is 2000 mm. The adjacent cables in the first row are connected by the W steel belt (the belt is parallel to the roadway trend). The gangue side is supported by a "single hydraulic prop + 11#joist steel + steel mesh." The spacing of single prop is 600 mm, the spacing of joist steel is 600 mm, and the spacing is evenly arranged. The reinforcing mesh is tied with joist steel, and the size of reinforcing mesh is 2300 mm × 800 mm. The embedded joist steel is more than 300 mm below the floor.

4. Numerical Simulation in Two Modes

4.1. Model Establishment. To examine the evolution law of displacement and stress of the surrounding rock under the two mining technologies further, Flac3D numerical software was used to perform simulation research based on actual field dimensions [28]. Figure 12(a) shows the established numerical model with dimensions of 200 m × 80 m × 50 m (length × width × height). Figures 12(b) and 12(c) show the arrangement of rock layers and model boundary conditions under two mining conditions. The Mohr-Coulomb model was used as the constitutive model of the rock mass. The empty element model was used to simulate roadway driving and working face mining. Both models are constrained by the displacement boundary. The velocity of the front and rear boundary along the y direction was set as 0, velocity of left and right boundary along the x direction was set as 0, velocity of bottom boundary along the x, y, and z directions was set as 0, the upper boundary corresponds to a free surface, and the weight load of the overlying strata is 12.5 MPa.

4.2. Simulation Results

4.2.1. Law of Stress Evolution. Figures 13(a) and 13(b) and Table 1 show the distribution of vertical stress when the working face is excavated at 40 m. Figure 13(c) shows the distribution of vertical stress of a 30 m lagging working face. Figure 13(d) shows the advance stress distribution 5 m ahead of the working face. As shown in the stress distribution, a certain stress concentration area is formed in front of the working face while a stress reduction area is formed under the condition of roof cutting. Based on Figure 13(c), the peak value of side abutment pressure is 20.54 MPa under the traditional GSER and 18.24 MPa under the roof cutting, and the stress decreases by approximately 12%. Furthermore, a stress concentration zone is formed at the filling body, and the maximum stress is 4.94 MPa. Based on Figure 13(d), the advance stress under the condition of roof cutting is generally lower than that of the traditional mode. This is due to the roof cutting that causes the overlying roof of the solid coal side to change from the fixed end to the simply supported end.

4.2.2. Analysis on the Deformation of Retained Roadway. Figure 14 shows the deformation monitoring. Figure 14(a) shows the deformation curve under traditional conditions. Figure 14(b) shows the curve under roof cutting. As shown in the curve analysis, the deformation of filling body and roof of the traditional reserved roadway is relatively evident. The maximum horizontal displacement of point B is

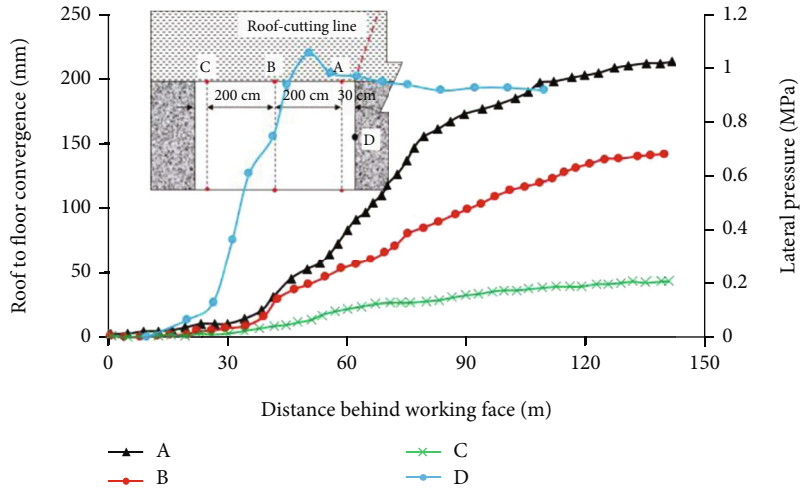

(a)

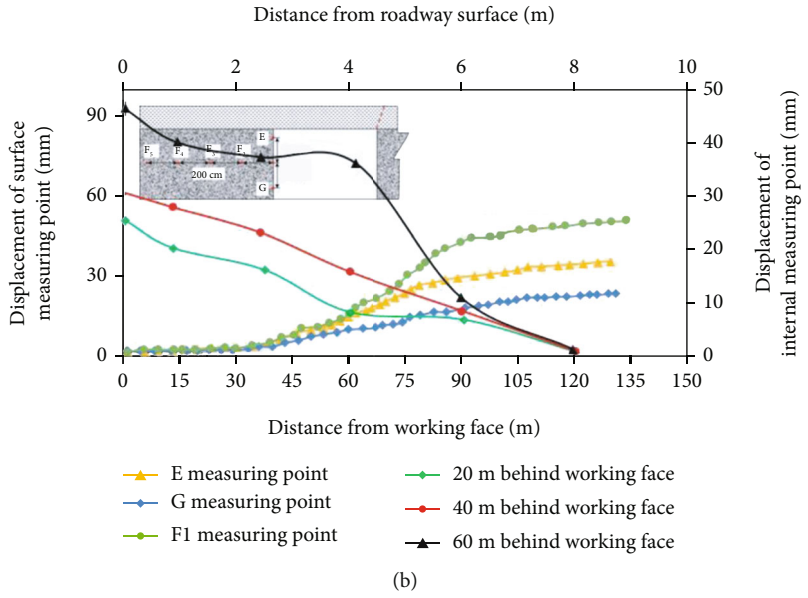

(b)

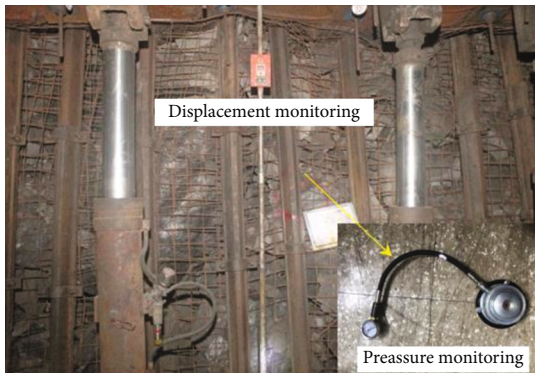

(c)

(d)

Figure 15: Deformation monitoring of surrounding rock: (a) roof to floor convergence, (b) roadway rib displacement, (c) layout of displacement monitoring, and (d) effect of retained roadway.

830 mm; the maximum vertical displacement of point *A* in the middle of the roof is 710 mm. The deformation of solid coal and floor is low, and the maximum horizontal displacement of *D* is 340 mm. The maximum vertical deformation of the floor is 220 mm, and the overall deformation of the retained roadway is relatively large. When compared with the traditional GSER, the deformation under the condition of roof cutting decreases as a whole. The maximum vertical

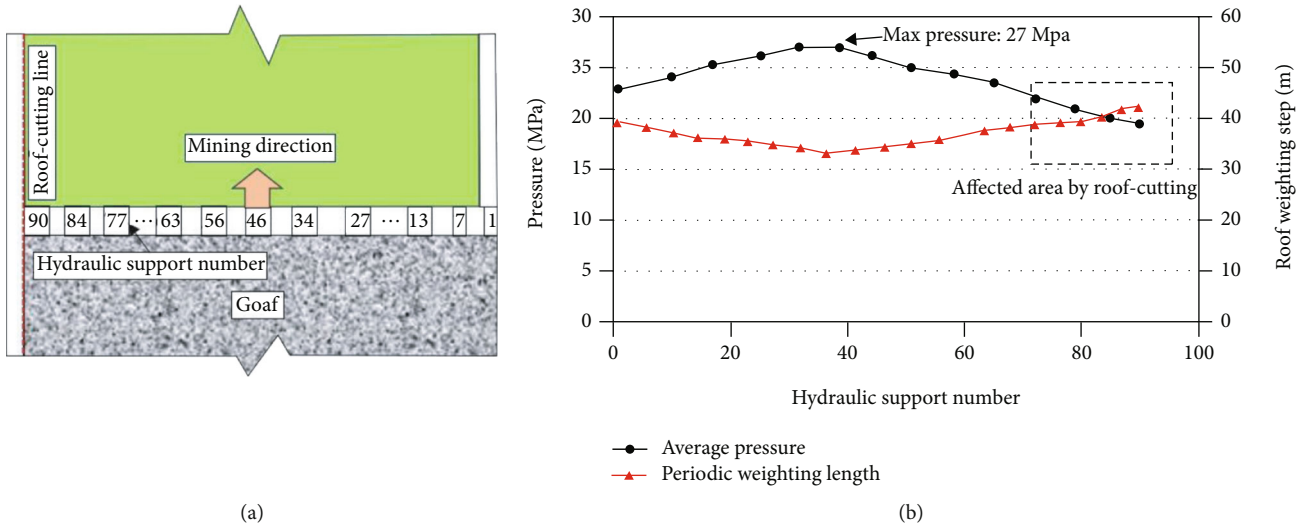

Figure 16: Mine pressure monitoring: (a) layout of hydraulic support; (b) distribution law of mine pressure.

displacement of the roof is 310 mm, which is located at the roof-cutting side. On the right side of the roadway, the deformation is considered zero due to the measures of retaining gangue on site. The floor heave is concentrated on the right side of the middle, with a maximum of 370 mm. The displacement of the two sides is low, and the overall deformation decreases by approximately 50%. Therefore, the effect of a retaining roadway is better than that of traditional conditions.

The simulation analysis indicated that the roof cutting fractures the load transfer articulated beam structure formed by the overlying hard and thick roof. The stress cannot be transferred to the retained roadway side, and thus, the stress distribution of the surrounding rock is optimized. However, the structure is not changed by the traditional GSER. Hence, the stress value in the traditional mode exceeds that under the condition of roof cutting, and the surrounding rock deformation also increases.

5. On-Site Monitoring

To analyze the stability of the tunnel and working face quantitatively (which adopt the roof-cutting-type GSER), the engineering application effect is evaluated via the deformation monitoring of the retained roadway and stress monitoring of the hydraulic support of the working face.

5.1. Tunnel Deformation Monitoring. Figure 15(a) shows the monitoring curve of the roof to floor convergence and the lateral gangue retaining pressure. The layout of the monitoring instrument is shown in Figure 15(c). Based on the curve, the deformation is low when the monitoring section is within 30 m from the working face. The displacement increases sharply when the distance from the working face exceeds 30 m. When the monitoring section lags 80 m behind the working face, the roof stratum movement tends to be gentle and the deformation rate is low. The convergence of monitoring point A on the roof-cutting side corresponds to the largest deformation of 210 mm while monitoring point C at the solid coal side exhibits the lowest deformation of 40 mm. Point D denotes the monitoring of the horizontal thrust of the gangue retaining facilities. As shown in the curve, the horizontal thrust increases rapidly when it is 27 m away from the working face, and it tends to be stable after reaching 60 m, and the pressure value is stable at approximately 0.9 MPa. The rapid increase stage of pressure essentially corresponds to the increase stage of convergence. Figure 15(b) shows the displacement curve of the solid coal side. The deformation trend of the surface measuring points is consistent with that of the roof although the deformation value is low. The internal measuring points of solid coal decrease with increases in the distance from the external surface, and the deformation is zero when the distance is 8 m.

5.2. Distribution Characteristics of Mine Pressure. As shown in Figure 16(a), 90 hydraulic supports are arranged on the working face, and they are numbered from the right side. With advances in the working face, the stress of the hydraulic support is monitored in real time, and the change rule of the periodic weighting interval along the inclined direction of the working face is analyzed, as shown in Figure 16(b). As shown in the curve analysis, the average stress of the hydraulic support in the middle of the working face corresponds to the highest stress, and the periodic weighting interval corresponds to the shortest length. The average stress of the hydraulic support on the roof side is lower than that on the uncut side, and its periodic weighting interval exceeds that on the uncut side. This is because the roof cutting causes the overlying roof strata on the cutting side to change from the fixed support state to the simple support state such that the roof breaking law in a certain range changes. As shown in the comparison, the transverse influence range of the working face is approximately 29.75 m due to roof cutting.

6. Conclusion

In this study, the roadway deformation and failure problems under the condition of traditional GSER with hard thick roof

were examined, and the failure mechanism was investigated. The improvement measures of roof-cutting-type GSER was proposed, and the principle of the main technology process was analyzed in detail. The comparative analysis of two technologies was performed via numerical simulation, and the effect of roadway retaining was evaluated via on-site monitoring. The following conclusions were obtained:

(1) The mechanical model under the traditional GSER was established and solved. Four kinds of deformation causes were obtained: (1) the hard thick roof rotates and sinks; (2) the mining height is high, the filling height of the collapsed gangue is low, and this creates favorable conditions for the subsidence of the main roof; (3) the large section of the roadway; and (4) the periodic fracture of hard thick roof

(2) Based on the four deformation causes, the roof-cutting-type GSER technology was proposed and the principle was analyzed; i.e., via roof cutting, the articulated beam structure formed by the overlying strata is cut off, stress transfer path is cut off, stress distribution is optimized, and the deformation of the surrounding rock also decreases

(3) The numerical simulation results indicate that a certain range of stress concentration area exists on the retained roadway side under the condition of traditional GSER while a certain range of stress reduction area is generated under the condition of roof cutting. This is conducive to the roadway stability. The peak value of lateral abutment pressure reduced from 20.54 MPa (under the traditional condition) to 18.2 MPa under the condition of roof cutting, which was a decrease of approximately 12%

(4) The field monitoring results indicated that under the condition of roof cutting, the roadway deformation was the most severe in the range of 30–80 m behind the working face, the deformation was gradually stable after 80 m. The variation trend of lateral pressure was similar to the convergence. Along the inclined direction of the working face, the average stress of the hydraulic support corresponded to the highest in the middle part, which was followed by the uncut side. The pressure value on the roof-cutting side was the lowest, and the periodic weighting length on the cutting side corresponded to the highest

Data Availability

The data used to support the findings of this study are available from the corresponding author upon request.

Conflicts of Interest

The authors declare that there is no conflict of interest regarding the publication of this paper.

Acknowledgments

This study received financial support from the special funds from the National Natural Science Foundation of China (No. 51574248).

References

[1] H. Yavuz, "An estimation method for cover pressure re-establishment distance and pressure distribution in the goaf of longwall coal mines," *International Journal of Rock Mechanics and Mining Sciences*, vol. 41, no. 2, pp. 193–205, 2004.

[2] N. Deisman, M. Khajeh, and R. J. Chalaturnyk, "Using geological strength index (GSI) to model uncertainty in rock mass properties of coal for CBM/ECBM reservoir geomechanics," *International Journal of Coal Geology*, vol. 112, pp. 76–86, 2013.

[3] J. B. Bai, W. L. Shen, G. L. Guo, X. Y. Wang, and Y. Yu, "Roof deformation, failure characteristics, and preventive techniques of gob-side entry driving heading adjacent to the advancing working face," *Rock Mechanics and Rock Engineering*, vol. 48, no. 6, pp. 2447–2458, 2015.

[4] R. Bertuzzi, K. Douglas, and G. Mostyn, "An approach to model the strength of coal pillars," *International Journal of Rock Mechanics and Mining Sciences*, vol. 89, pp. 165–175, 2016.

[5] J. Ning, J. Wang, T. Bu, S. Hu, and X. Liu, "An innovative support structure for gob-side entry retention in steep coal seam mining," *Minerals*, vol. 7, no. 5, pp. 1–18, 2017.

[6] A. Azadeh, M. Osanloo, and M. Ataei, "A new approach to mining method selection based on modifying the Nicholas technique," *Applied Soft Computing*, vol. 10, pp. 1040–1061, 2010.

[7] C. O. Karacan, "Prediction of porosity and permeability of caved zone in longwall gobs," *Transport in Porous Media*, vol. 82, no. 2, pp. 413–439, 2010.

[8] Q. Bai, S. Tu, F. Wang, and C. Zhang, "Field and numerical investigations of gateroad system failure induced by hard roofs in a longwall top coal caving face," *International Journal of Coal Geology*, vol. 173, pp. 176–199, 2017.

[9] Y. L. Tan, F. H. Yu, J. G. Ning, and T. B. Zhao, "Design and construction of entry retaining wall along a gob side under hard roof stratum," *International Journal of Rock Mechanics and Mining Sciences*, vol. 77, pp. 115–121, 2015.

[10] C. Han, N. Zhang, J. Xue, J. Kan, and Y. Zhao, "Multiple and long-term disturbance of gob-side entry retaining by grouped roof collapse and an innovative adaptive technology," *Rock Mechanics and Rock Engineering*, vol. 52, no. 8, pp. 2761–2773, 2019.

[11] P. Wang, L. Jiang, J. Jiang, P. Zheng, and W. Li, "Strata behaviors and rock-burst-inducing mechanism under the coupling effect of a hard thick stratum and a normal fault," *International Journal of Geomechanics*, vol. 18, no. 2, pp. 1–14, 2018.

[12] J. Coggan, F. Gao, D. Stead, and D. Elmo, "Numerical modelling of the effects of weak immediate roof lithology on coal mine roadway stability," *International Journal of Coal Geology*, vol. 90, pp. 100–109, 2012.

[13] D. W. Yang, Z. G. Ma, F. Z. Qi et al., "Optimization study on roof break direction of gob-side entry retaining by roof break and filling in thick-layer soft rock layer," *Geomechanics and Engineering*, vol. 13, no. 2, pp. 195–215, 2017.

[14] Q. Wang, M. He, J. Yang, H. Gao, B. Jiang, and H. Yu, "Study of a no-pillar mining technique with automatically formed gob-side entry retaining for longwall mining in coal mines," *International Journal of Rock Mechanics and Mining Sciences*, vol. 110, pp. 1–8, 2018.

[15] Q. Wang, Q. Qin, and B. Jiang, "Study and engineering application on the bolt-grouting reinforcement effect in underground engineering with fractured surrounding rock," *Tunnelling and Underground Space Technology*, vol. 84, pp. 237–247, 2019.

[16] V. M. Seryakov, S. V. Rib, and V. N. Fryanov, "Stress state of a coal pillar in fully mechanized longwall mining in dislocation zone," *Journal of Mining Science*, vol. 53, no. 6, pp. 1001–1008, 2017.

[17] M. He, Y. Gao, J. Yang, and W. Gong, "An innovative approach for gob-side entry retaining in thick coal seam longwall mining," *Energies*, vol. 10, no. 11, pp. 1–22, 2017.

[18] Z. Ma, J. Wang, M. He, Y. Gao, J. Hu, and Q. Wang, "Key technologies and application test of an innovative noncoal pillar mining approach: a case study," *Energies*, vol. 11, no. 10, pp. 1–22, 2018.

[19] Y. Gao, Y. Wang, J. Yang, X. Zhang, and M. He, "Meso- and macroeffects of roof split blasting on the stability of gateroad surroundings in an innovative nonpillar mining method," *Tunnelling and Underground Space Technology*, vol. 90, pp. 99–118, 2019.

[20] L. Jiang, P. Wang, P. Zheng, H. Luan, and C. Zhang, "Influence of different advancing directions on mining effect caused by a fault," *Advances in Civil Engineering*, vol. 2019, Article ID 7306850, 10 pages, 2019.

[21] F. A. Ooriad, M. Yari, R. Bagherpour, and M. Khoshouei, "The development of a novel model for mining method selection in a fuzzy environment; case study; Tazareh coal mine, Semnan Province, Iran," *Rudarsko-geološko-naftni zbornik (The Mining-Geological-Petroleum Engineering Bulletin)*, vol. 33, no. 1, pp. 45–53, 2018.

[22] J. Wang, W. Li, D. Y. Zhu, W. Gong, and Y. Su, "Novel application of the roof-cutting-type gob-side entry retaining in coal mine," *Mathematical Problems in Engineering*, vol. 2021, Article ID 1625282, 16 pages, 2021.

[23] A. S. Ranathunga, M. S. Perera, and P. G. Ranjith, "Deep coal seams as a greener energy source: a review," *Journal of Geophysics and Engineering*, vol. 11, no. 6, pp. 630–647, 2014.

[24] Z. B. Guo, Q. Wang, H. H. Wang, Z. M. Ma, and H. L. Hu, "Analysis of the swelling characteristics and lateral pressure of the mudstone in the rubble side of the cut top lane," *Journal of China University of mining and Technology*, vol. 47, no. 5, pp. 987–994, 2018.

[25] G. Li, F. S. Ma, J. Guo, H. Zhao, and G. Liu, "Study on deformation failure mechanism and support technology of deep soft rock roadway," *Engineering Geology*, vol. 264, article 105262, 2020.

[26] D. Huang and Y. Li, "Strength and Failure of mechanism of brittle rocks under tensile-compressive ressive stress state with partical flow simulation," *Journal of Engineering Geology*, vol. 28, no. 4, pp. 677–684, 2020.

[27] D. Denise and F. Quevedo, "Analytical solution of deep tunnels in a strain-hardening elasto-plastic rock mass," *Latin American Journal of Solids and Structures*, vol. 17, no. 6, article e297, 2020.

[28] S. R. Islavath, D. Deb, and H. Kumar, "Numerical analysis of a longwall mining cycle and development of a composite longwall index," *International Journal of Rock Mechanics and Mining Sciences*, vol. 89, pp. 43–54, 2016.